Article:
He, F., Sarrigiannis, P.G., Billings, S.A. et al. (2016) Nonlinear interactions in the thalamocortical loop in essential tremor: A model-based frequency domain analysis. Neuroscience, 324. pp. 377-389. ISSN: 0306-4522

https://doi.org/10.1016/j.neuroscience.2016.03.028

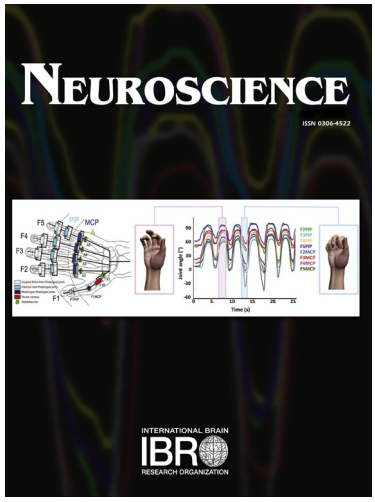

Nonlinear interactions in the thalamocortical loop in essential tremor: a model-based frequency domain analysis

Fei He, Ptolemaios G. Sarrigiannis, Stephen A. Billings, Hualiang Wei, Jeremy Rowe, Charles Romanowski, Nigel Hoggard, Marios Hadjivassilliou, Dasappaiah Ganesh Rao, Richard Grünewald, Aijaz Khan, John Yianni

PII: S0306-4522(16)00251-7
DOI: http://dx.doi.org/10.1016/j.neuroscience.2016.03.028
Reference: NSC 16992

To appear in: *Neuroscience*

Accepted Date: 8 March 2016

Please cite this article as: F. He, P.G. Sarrigiannis, S.A. Billings, H. Wei, J. Rowe, C. Romanowski, N. Hoggard, M. Hadjivassilliou, D.G. Rao, R. Grünewald, A. Khan, J. Yianni, Nonlinear interactions in the thalamocortical loop in essential tremor: a model-based frequency domain analysis, *Neuroscience* (2016), doi: http://dx.doi.org/10.1016/j.neuroscience.2016.03.028

Nonlinear interactions in the thalamocortical loop in essential tremor: a model-based frequency domain analysis

Fei He [a,*], Ptolemaios G. Sarrigiannis [b,*], Stephen A. Billings [a], Hualiang Wei [a], Jeremy Rowe [c], Charles Romanowski [e], Nigel Hoggard [e], Marios Hadjivassilliou [f], Dasappaiah Ganesh Rao [b], Richard Grünewald [f], Aijaz Khan [f], John Yianni [c]

[a]Department of Automatic Control and Systems Engineering, University of Sheffield, S1 3JD, United Kingdom
[b]Department of Clinical Neurophysiology, Sheffield Teaching Hospitals NHS Foundation Trust, Royal Hallamshire Hospital, Sheffield, S10 2JF, United Kingdom
[c]Department of Neurosurgery, Sheffield Teaching Hospitals NHS Foundation Trust, Royal Hallamshire Hospital, Sheffield, S10 2JF, United Kingdom
[e]Department of Radiology, Sheffield Teaching Hospitals NHS Foundation Trust, Royal Hallamshire Hospital, Sheffield, S10 2JF, United Kingdom
[f]Department of Neurology, Sheffield Teaching Hospitals NHS Foundation Trust, Royal Hallamshire Hospital, Sheffield, S10 2JF, United Kingdom

Authors e-mails: f.he@sheffield.ac.uk, ptolemaios.sarrigiannis@sth.nhs.uk, s.billings@sheffield.ac.uk, w.hualiang@sheffield.ac.uk, Jeremy.Rowe@sth.nhs.uk, Charles.Romanowski@sth.nhs.uk, Nigel.Hoggard@sth.nhs.uk, Marios.Hadjivassiliou@sth.nhs.uk, Ganesh.Rao@sth.nhs.uk, Richard.Grunewald@sth.nhs.uk, Aijaz.Khan@sth.nhs.uk, John.Yianni@sth.nhs.uk,

Corresponding authors:
Fei He, Department of Automatic Control and Systems Engineering, University of Sheffield, S1 3JD, United Kingdom. Email: f.he@sheffield.ac.uk,
Ptolemaios G Sarrigiannis, Department of Clinical Neurophysiology, N Floor, Sheffield Teaching Hospitals NHS Foundation Trust, Royal Hallamshire Hospital, Sheffield, S10 2JF, United Kingdom. Email: ptolemaios.sarrigiannis@sth.nhs.uk, p.sarrigiannis@sheffield.ac.uk,

Abstract

There is increasing evidence to suggest that essential tremor has a central origin. Different structures appear to be part of the central tremorogenic network, including the motor cortex, the thalamus and the cerebellum. Some studies using EEG and MEG show linear association in the tremor frequency between the motor cortex and the contralateral tremor EMG. Additionally, high thalamomuscular coherence is found with the use of thalamic local field potential (LFP) recordings and tremulous EMG in patients undergoing surgery for deep brain stimulation (DBS). Despite a well-established reciprocal anatomical connection between thalamus and cortex, the functional association between the two structures during "tremor-on" periods remains elusive. Coherence analysis shows strong linear association between thalamic LFPs and contralateral tremor EMG, but the relationship between the EEG and the thalamus is much less clear. Thalamic (Vim) LFPs, ipsilateral scalp EEG from the sensorimotor cortex and contralateral tremor arm EMG recordings were obtained from two patients with essential tremor who had undergone successful surgery for DBS. These measurements were then analysed by constructing a novel parametric nonlinear autoregressive exogenous model (NARX). This new approach uncovered two distinct and not overlapping frequency "channels" of communication between Vim thalamus and the ipsilateral motor cortex, defining robustly "tremor-on" versus "tremor-off" states. The associated estimated nonlinear time lags also showed non-overlapping values between the two states, with longer corticothalamic lags (exceeding 50ms) in the tremor active state, suggesting involvement of an indirect multisynaptic loop. The results reveal the importance of the nonlinear interactions between cortical and subcortical areas in the central motor network of essential tremor. This work is important because it demonstrates for the first time that in essential tremor the functional interrelationships between cortex and thalamus should not be sought exclusively within individual frequencies but more importantly between cross-frequency nonlinear interactions. Should our results be successfully reproduced on a bigger cohort of patients with essential tremor, our approach could be used to create an on-demand closed-loop DBS device, able to automatically activate when the tremor is on.

Key words: Nonlinear modelling, spectral analysis, coherence, EEG, local field potentials, essential tremor

Highlights

- We use a nonlinear autoregressive exogenous model to de-codify corticothalamic communication
- We reveal nonlinear interactions between motor cortex and thalamus in essential tremor
- We define corticothalamic interactions during tremor active and rest states
- There are state specific frequencies and time lags in corticothalamic interrelationships

1. Introduction

Essential tremor is a common neurological movement disorder considered to be a centrally driven tremor. The central oscillating constituents of the network comprise parts of the physiological central motor system (Raethjen and Deuschl, 2012). There is both neurophysiological and clinical evidence of thalamic involvement in the central oscillatory network generating essential tremor (Hirai et al., 1983, Hubble et al., 1996, Marsden et al., 2000, Vaillancourt et al., 2003, Lyons and Pahwa, 2004, Hua and Lenz, 2005, Deuschl et al., 2011). Local field potential (LFP) recordings of thalamic ventralis intermedius (Vim) nucleus show strong linear correlation with the contralateral EMG during tremor (Marsden et al., 2000). Besides this, there is evidence suggesting the sensorimotor cortex is part of this central tremor related oscillatory network with significant coupling in some cases between the primary motor cortex (M1) and the contralateral tremorogenic EMG (Hellwig et al., 2000, Hellwig et al., 2001, Hellwig et al., 2003, Govindan et al., 2006, Schnitzler et al., 2009, Muthuraman et al., 2012, Raethjen and Deuschl, 2012). However, this was not a universal finding and negative results were also reported (Halliday et al., 2000). There is also some suggestion that the constituents of the central motor network are not fixed but vary over time with the motor cortex being intermittently involved in the tremor generation (Raethjen et al., 2007, Raethjen and Deuschl, 2012). Looking now into the communication between the thalamus and the cortex, it is well established that there are strong reciprocal anatomical connections between cortex and thalamus (Jones, 2007, Zhang et al., 2008). Nonetheless, interactions between thalamus and cortex, although previously reported during essential tremor (Marsden et al., 2000), have not to our knowledge been extensively defined although equally strong flow of information in both directions has been reported (Raethjen and Deuschl, 2012). This latter work is based on scalp EEG recordings and not on thalamic LFPs.

In particular, it is not clear yet if there is a specific range of frequencies at which the cerebellar thalamus and cortex interact when essential tremor is activated and if this is any different to the resting state communications. These are important and challenging problems that will be investigated in this study.

It has long been suggested that neuronal networks already at a cellular level and based on phenomena of integration, threshold and saturation demonstrate strong nonlinear dynamic behaviour (Lehnertz, 2008). Although the author made these observations with epilepsy in mind, these are ubiquitous neuronal cellular mechanisms. In light of this, it is hard to imagine that the central oscillatory network in tremors, thought to involve cortical and complex multisynaptic subcortical areas, can be sufficiently explored based exclusively on linear association methods such as coherence, commonly used in this field.

In this study, we introduce a parametric nonlinear autoregressive with exogenous variable (NARX) frequency domain model to assess the corticothalamic interactions between the LFPs recorded from the thalamus (Vim) and the activity from the motor cortex recorded with scalp EEG electrodes on the opposite side of the tremor recorded on EMG. We demonstrate that this novel method can robustly distinguish between periods of "tremor-on" versus "tremor-off'. We show with reference to two patients with essential tremor, who underwent successful surgery for deep brain stimulation (DBS), that the interactions between Vim thalamus and cortex during tremor and resting states occur at non-overlapping frequency and time lag ranges. The results of classical non-parametric higher-order spectral (i.e. bispectral) analysis of thalamic LFPs during both brain states are also provided for comparison. We will show evidence of the importance of cross frequency nonlinear interactions, between cortex and thalamus, in essential tremor.

2. Experimental procedures

2.1. Patients

We present data recorded and analysed from 2 patients (64 and 60 year old females) with essential tremor who underwent deep brain stimulation surgery for their condition. Both cases had postural tremor that persisted during movement but no dysmetria. Their dominant, right upper limb was more affected and this side was used for our study. Neither patient had a family history for tremor. The Fahn-Tolosa-Marin tremor rating scale was used for the pre- and post-operative assessments. Essential demographic and other pre- and post-operative parameters are included in Table 1.

2.2. Surgical procedures

Surgery was performed under local anaesthesia, using the CRW frame, targeting the thalamus with previously acquired MRI scans fused to a stereotactic CT scan. A more detailed account of the surgical methodology employed has been described previously (Papanastassiou et al., 1998, Orth et al., 1999). Bilateral Vim thalamic nuclei were implanted with Medtronic 3387 electrodes and their positions confirmed with stereotactic CT imaging. The target points were also related to the mid commissural point (MCP) as follows: Vim 12mm lateral and 4mm posterior to the MCP. The implanted electrodes were externalised for a period of trial stimulation using Medtronic test stimulator (ENS), following which the electrodes were internalised and connected to an Activa RC implantable pulse generator (Medtronic Inc.). Optimal lead placement for tremor suppression was achieved with the aid of intraoperative stimulation.

2.3. Electrophysiological recordings

Our current clinical practice incorporates electrophysiological polygraphy recordings in patients with tremor undergoing DBS surgery while trialling various parameters of stimulation. EEG/EMG polygraphy recordings with thalamic LFPs were performed with the Xltek EMU 128 headbox (Optima Medical Ltd) with a sampling rate at 2000Hz five days after surgery and while the implanted electrodes were externalised in both patients. Standard 10-20 international system of electrode placement positions were used for the EEG recordings with a linked earlobe reference. In this work we have used bipolar frontocentral derivations (F3C3 and F4C4) for our analysis. Ethics approval to use EEG/polygraphy recordings and local field potentials (LFPs) to develop new methods and techniques has been granted both from the University of Sheffield and the NHS ethics committees (SMBRER207 and 11/YH/0414).

2.4. Data processing

Data was exported in Spike 2 (version 8.03) software and high pass filtered at 0.8 Hz and then down-sampled from 2000Hz to 500Hz for nonparametric coherence and bispectral analysis and to 100Hz for parametric modelling based analysis. The EMG data was rectified. Two relatively artefact free 4-second epochs of EEG, Thalamic LFPs and EMG for “tremor-on” and two for “tremor-off” states were isolated for both patients and used for the analysis. Data was exported in text format and Matlab (version 2014a) was then used for all the

remaining quantitative signal analysis and model construction. We use thalamic LFPs recorded between the most rostral and caudal electrode contacts for the purpose of our analysis (contact 0 active and 3 as reference).

2.5. Spectral and coherence analysis

The linear dependence between two signals in the frequency domain is usually measured by the spectral coherence. The coherence between two signals $x(t)$ and $y(t)$, $t = 1, 2,\ldots, N$, at frequency f is defined as:

$$C_{xy}(f) = \frac{\left|S_{xy}(f)\right|^2}{S_{xx}(f)S_{yy}(f)} \quad (1)$$

where $S_{xy}(f)$ is the cross-spectral density between x and y, and $S_{xx}(f)$ and $S_{yy}(f)$ the auto-spectral density of x and y respectively. The cross-spectral and auto-spectral densities are normally the Fourier transforms of the cross-correlation and auto-correlation functions of the two signals. Values of coherence will always between 0 and 1. A value of $C_{xy}(f)$ less than one indicates either the measurements is corrupted by noise or there exist nonlinear relationships between these two signals. The significance level of coherences can be estimated by using a bootstrap algorithm. One of the time series is re-ordered randomly (the resulting series should have no correlation with the original and other series) and the coherence is re-computed. This procedure is performed a large number of times and a distribution of coherences for all frequencies are obtained, from which a (e.g. 95%) significance level is derived.

2.6. Bispectral analysis

Since power spectra and coherence are based on Fourier transforms of the auto- and cross-correlations of signals, they are only linear frequency domain measures. Practically these measures can be completely blind to certain nonlinear effects or correlations such as quadratic moments in and between signals that have a zero mean (Billings, 2013). Higher-order spectral analysis has then been proposed to detect nonlinear correlations between spectral components. The most widely used is the bispectral analysis (Nikias and Raghuveer, 1987) that transforms third-order statistics from the time to the frequency domain, and the quadratic nonlinear interactions such as quadratic phase coupling (QPC) can be detected and quantified. Bispectral analysis has recently been applied to study the nonlinear correlations between different frequency components (rhythms) in the subthalamic LFPs related to

Parkinson's disease, including during tremor (Marceglia et al., 2006b, Wang et al., 2014). The bispectrum of a signal $y(t)$ is defined as:

$$B(f_1,f_2)=\mathcal{F}\{\gamma(k_1,k_2)\}=\sum_{m_1=-\infty}^{+\infty}\sum_{m_2=-\infty}^{+\infty}\gamma(k_1,k_2)e^{-j2\pi(f_1k_1+f_2k_2)}$$
$$\gamma(k_1,k_2)=E[y(t)y(t+k_1)y(t+k_2)] \quad (2)$$

Where f_1 and f_2 are the 2-dimensional frequencies, $\mathcal{F}\{\cdot\}$ denotes the Fourier transformation, $\gamma(k_1,k_2)$ is the third-order cumulant with time lags k_1 and k_2. Non-parametric (i.e. direct and indirect methods) and parametric (e.g. AR/ARMA model based methods) based approaches were proposed to estimate the bispectrum, and both approaches have their advantages and disadvantages. In this work, the indirect nonparametric method is employed for the bispectrum estimation. The time lags selection is often case dependent and in our case studies at least 0.2 second time lags are used to ensure a good resolution to separate close peaks in the bispectrum estimates.

Similar to the cross-spectrum and coherence, the normalized bispectrum is named the bicoherence. Practically although a bicoherence measure can avoid the influence of large spectral amplitude, it can sometimes produce misleading results since insignificant bispectral peaks can become significant due to the normalization. To identify both frequency and phase coupling in the LFPs accurately and ensure the statistical significance, a surrogate data method (Theiler et al., 1992) is combined with the bispectrum estimation in this work and its superiority to a standard bicoherence index has been reported (Siu et al., 2008). Surrogate data are produced by randomizing the phase of the original data set. A surrogate data sequence has the same power spectrum and other linear statistical properties (e.g. mean, variance) as the original sequence, but it eliminates nonlinear properties (i.e. phase couplings). In this work, a large number (e.g. 100) of surrogate data of the original sequence are generated first. The 95% statistical threshold values are defined as the mean of all the surrogates' bispectral estimates plus twice its standard deviations. Only the bispectrum values that are larger than the threshold are considered significant and are displayed in the bispectrum results.

2.7. Nonlinear time and frequency domain analysis using NARX models

Although higher-order spectral (e.g. bispectral) analysis can be used to detect nonlinear effects in signals, the corresponding non-parametric estimation normally requires large data sets and the windowing and smoothing in multi-dimensions are complicated and computationally expensive. In addition, bispectral analysis is mainly used as a univariate analysis approach and cannot indicate whether a nonlinear interaction, e.g. quadratic phase coupling, is introduced from a specific signal of interest, nor can it reveal the underlying temporal nonlinear relationships which can be valuable in interpretation. To analyse the nonlinear interactions between LFP and EEG recordings, a more robust and high resolution nonlinear frequency domain approach is required.

In this work, a well-known nonlinear parametric model, the NARX model (Leontaritis and Billings, 1985, Billings, 2013), is first employed to model both the linear and nonlinear interactions between EEG and thalamic LFP in the time domain, and it is then mapped to the frequency domain to reveal the interactions of different frequency components in both signals. Consider two signals (or stochastic processes) with discrete time observations $x(t)$ and $y(t)$, $t = 1, 2,\ldots, N$. The polynomial NARX model with respect to y can be expressed as

$$y(t) = \sum_{n=1}^{M} \sum_{p=0}^{n} \sum_{k_1,\ldots,k_{p+q}=1}^{K} c_{p,q}(k_1,\ldots,k_{p+q}) \times \prod_{i=1}^{p} y(t-k_i) \prod_{i=p+1}^{p+q} x(t-k_i) + \xi(t) \tag{3}$$

where n denotes the n^{th}-order nonlinearity of the system with a maximum order of M; and $p + q = n$, $k_i = 1,\ldots,K$, $\sum_{k_1,k_{p+q}=1}^{K} \equiv \sum_{k_1=1}^{K} \cdots \sum_{k_{p+q}=1}^{K}$. The number of model terms increases as the order of input and output terms (q and p) and the corresponding maximum lags (K) increase. $\xi(t)$ is the model prediction error or a noise sequence that is assumed zero mean and independent. The NARX models can typically be identified based on the forward regression with orthogonal least squares (FROLS) method (Billings et al., 1989, Chen et al., 1989). By using the FROLS algorithm, a "best" model structure, i.e. the linear and nonlinear regressors, is selected and the model complexity is controlled to avoid over fitting, and the model parameters are estimated. In addition, if the system under study is linear, the FROLS method automatically discards the nonlinear terms and only estimates a linear model. In cases where the system under study is stochastic with unknown coloured noise, noise models should be employed to form a NARMAX model (Billings, 2013, He et al., 2015).

The identified model can be statistically validated using the correlation tests (Billings and Voon, 1983). Five cross-correlation functions, i.e. $\phi_{\xi\xi}(\tau)$, $\phi_{x\xi}(\tau)$, $\phi_{\xi(\xi x)}(\tau)$, $\phi_{(x^2)'\xi}$, and $\phi_{(x^2)'\xi^2}$ (with model residual ξ and $(x^2)'$ a zero-mean process of x^2), are used in conjunction with

95% confidence intervals (approximately $\pm 1.96/\sqrt{N}$) to test whether the residuals are uncorrelated with all linear and nonlinear combinations of past inputs, outputs and residuals. This validation routine is applied to examples in this paper.

The frequency domain analysis of a nonlinear system is much more complicated, and is mainly based on the concept of generalized frequency response functions (GFRFs) that extend the linear FRF to higher orders and dimensions. Following the derivations in (Lang and Billings, 1996, Billings, 2013) the output spectrum of a nonlinear system can be formulated using the output frequency response function (OFRF)

$$Y_{ylx}(f) = \sum_{n=1}^{M} \left(\frac{1}{\sqrt{n}} \int_{f_1+\ldots+f_n=f} H_n(f_1,\ldots,f_n) \prod_{i=1}^{n} X(f_i) df \right) \tag{4}$$

Here, the nth-order GFRF $H_n(f_1,\ldots,f_n)$ was defined as the multiple Fourier transform of the nth-order Volterra kernel, and later extended to the NARX model cases (Billings and Tsang, 1989, Jones and Billings, 1989). For a NARX model, the corresponding nth-order GFRF can be expressed directly from the estimated time domain model parameters from (3) as

$$H_n(f_1,\ldots,f_n) = \frac{H_{n[x]}(f_1,\ldots,f_n) + H_{n[y]}(f_1,\ldots,f_n) + H_{n[xy]}(f_1,\ldots,f_n)}{1 - \sum_{k_1=1}^{K} c_{1,0}(k_1) e^{(-j2\pi(f_1+\ldots+f_n)k_1/f_s)}} \tag{5}$$

where the contributions of the pure input, output and cross-product nonlinearities, $H_{n[x]}$, $H_{n[y]}$, and $H_{n[xy]}$, are defined in the Appendix A. Hence the link between the temporal nonlinear model and the frequency response behaviours is revealed, this can be important in interpretation and is not possible where Fourier transform methods are applied.

The first-order GFRF describes the linear frequency response and only corresponds to the linear part of the nonlinear time-domain model (3). The 'peaks' in the first-order GFRF are similar to the 'resonance frequencies' of linear system and indicate at which frequencies the output response will be amplified. The gains of a second or a higher order GFRF would be in a high dimensional space and their maxima are the 'ridges' rather than 'peaks'. The locations of the 'ridges' indicate the transfer of energy from input spectral components to the output spectra at their summation, to produce nonlinear effects such as harmonics or intermodulation (He et al., 2013).

When a nonlinear model's GFRFs and input spectrum are available, the model's output frequency response can be calculated from (4). By comparing the model's OFRF with the output spectrum obtained from a classical nonparametric estimation such as FFT, an

independent validation of the model can often be provided in addition to the time-domain model validation discussed above.

2.8. Confidence intervals for the frequency response functions

Although the identified NARX model can be statistically validated using the correlation tests in the time domain, it is still important to examine the effects of time domain model parametric uncertainties to the model's frequency domain properties, i.e. the GFRFs. The 95% confidence intervals of the GFRFs can be computed by using a Monte Carlo approach (Worden, 1998). Since the polynomial NARX model (3) is linear-in-the-parameters and can be expressed in matrix form:

$$y(t) = \psi^T \theta + \xi(t) \tag{6}$$

where Ψ is the expanded regression matrix and $\theta = [c_{0,1}(1),\ldots,c_{0,1}(K),c_{1,0}(1),\ldots,c_{p,q}(K,\ldots,K)]^T$ is the parameter vector. Under the assumption that the residual signal ξ that contains both the measurement noise and modelling errors is zero-mean and Gaussian, the standard deviation for each estimated parameter can be expressed:

$$\sigma_i = \sigma_e \sqrt{[(\psi^T \psi)^{-1}]_{ii}} \tag{7}$$

The 95% confidence interval of parameter estimates become $\hat{\theta} \pm 1.96\sigma$ with $\hat{\theta}$ the nominal parameter estimates. This is an interval that with a 95% probability the true parameters can fall into. These time domain parametric uncertainties can then be mapped into the frequency response functions in the frequency domain, since an *n*th-order GFRF $H_n(f_1,\ldots,f_n)$ is only a function of the time domain model parameter values when the model structure is determined. By using a Monte Carlo sampling in the parametric uncertainty region $\hat{\theta} \pm 1.96\sigma$, the corresponding 95% confidence interval of an *n*th-order GFRF can be computed according to (5). It is important to note that the confidence bounds of a GFRF may not be symmetric to the nominal values as in the time domain case, because a GFRF is in a nonlinear relationship to the model parameters.

3. Results

3.1. DBS parameters and electrode placement

Both patients have experienced dramatic suppression of their tremor after DBS with the parameters described in Table 1. Imaging with pre-surgical fused MRI and CT scans and postsurgical CT scans have verified that the Vim electrodes were accurately placed. Therefore, the LFPs used in this study were recorded from anatomically and functionally ideally placed depth Vim electrodes.

3.2. EEG time series, spectral and coherence analysis

Two relatively artefact free 4-second epochs of electrophysiological recordings for "tremor -on" and two for "tremor-off" states were isolated for both patients and used for the analysis. Examples of the EEG, LFP and contralateral EMG recordings are shown in Fig. 1 and the corresponding spectral analysis in Fig. 2. Significant low frequency oscillations at 3-5Hz are observed in EMG recordings during the "tremor-on" state, and low frequency components below 5Hz are also observed in the thalamic LFPs during the tremor from the spectral analysis in both cases. In contrast, during "tremor-off" state low frequency oscillations in the EMG recordings disappear. The low frequency components (< 5Hz) in the LFPs are significantly reduced in magnitude, less than 0dB, compared with the "tremor-on" state and higher frequency components around 10 Hz are observed. The magnitude of EEG is also significantly reduced, but there is no clear difference in the peak of the frequencies between "tremor-on" and "tremor-off" states.

Coherences between pairs of cortical EEG, thalamic LFPs and contralateral EMG were computed according to (1) and shown in Fig. 3. Here, each 4-second recording is down-sampled to 500Hz and it has 2000 data samples. Hanning windows are employed with 50% overlap and 512 samples in each window. The number of averages then equals to $2\times2000/512 \approx 8$. The confidence level is computed from a bootstrap procedure as described in section 2.5. Of note is the lack of any substantial linear effects between frontal cortex and cerebellar thalamus when the tremor is on, although some coherence at low frequencies (within 10Hz) is observed but is not very significant compared with the confidence level (Fig. 3A and 3B). This is in sheer contrast with the high linear relationship between thalamus and tremulous EMG (Fig. 3C and 3D). Also the coherence between EEG and tremulous EMG is only borderline significant in the frequency range of the tremor in one of the two cases (Fig. 3E and 3F).

3.3. Bispectral analysis of thalamic Vim LFPs

The aforementioned epochs of Vim thalamic LFPs, from "tremor-on" and "tremor-off" states of both patients, were used to estimate bispectra and detect the quadratic phase coupling (QPC) under these two different brain states (Fig. 4). The original recordings were down-sampled to 500Hz. The indirect method was used to estimate bispectra with parameters setting as follows, 400 samples per segment, 100 time lags, 50% overlap, 512 points for FFT. The significance level of the bispectra estimation were tested using the surrogate approach described in Section 2.6.

These are unequivocally differentiated on simple inspection of the bispectra QPC graphs. Strong phase coupling at frequencies below 3Hz characterises the tremor active state, such as the peaks at (2.3Hz, 2.3Hz) for patient 1 and (1.7Hz, 1.7Hz) for patient 2 (Fig. 4A and 4C). Significant coupling around and above 5Hz is observed during the resting state, such as peaks at around (4Hz, 4Hz) in both two patients and extra peaks at (3Hz, 7.5Hz) and (7.5Hz, 3Hz) for patient 2 (as shown in Fig. 4B and 4D). These bispectra results also explain the variations of key frequency components in the power spectra of thalamic LFPs (as shown in Fig. 2), significant frequency components below 5Hz during tremor 'on' and higher frequency components around and above 10Hz during tremor 'off' which are actually the nonlinear (harmonics or inter-modulation) QPC effects. Other authors have found similar results in subthalamic LFPs in patients with Parkinson's disease (Marceglia et al., 2006a, López-Azcárate et al., 2010, Wang et al., 2014).

Apart from computational issues, bispectral analysis is mainly used as a univariate analysis approach and cannot indicate whether a nonlinear interaction, i.e. QPC, is introduced from a specific signal of interest. This is especially true when multiple peaks are observed as the case shown in the bispectrum of patient 2 thalamic LFP "tremor-off" state. Parametric NARX models and corresponding frequency domain analysis were then further applied to study the nonlinear interactions between cerebellar thalamus (LFP) and cortex (EEG).

3.4. Nonlinear modelling and frequency domain analysis

A bispectral result only shows the QPC at specific frequencies in a LFP recording, whilst the parametric NARX model based analysis presents a nonlinear system's properties between two signals, in this instance between the EEG and thalamic LFP. Such properties would indicate at which frequencies or combination of input frequencies the output frequency components would be amplified as a result of either linear or nonlinear effects quantitatively. As the thalamic LFP and not the EEG was shown before to present strong coherence with the

contralateral tremor EMG (Fig. 3C, 3D, 3E and 3F), which was also previously demonstrated by other authors (Marsden et al., 2000, Hua and Lenz, 2005), we have treated the EEG as the input and the LFP as the output to our NARX model in this study. Additionally, with this approach we avoid interactions from the sensory afferent peripheral feedback loop.

For parametric modelling, the original EEG and LFP data were down-sampled to 100Hz to ensure a relative simple but sufficient model to capture the nonlinear dynamics (see the OFRF analysis results below). NARX models with a maximum of third-order nonlinearity (n=3 in (3)) and maximum lags of 10 (K=10) in both input and output terms were used to model the interactions between EEG and LFP under different conditions. FROLS method was used to select appropriate linear and nonlinear model terms, and model parameters were estimated in the meantime. The first-, second- and third-order GFRFs (5) were then computed based on the identified NARX model. Since the third-order GFRF was very small in magnitude and did not show any significant contributions to the output frequency response, only the first- and second-order results were presented here. To visualize the second-order GFRFs in a two-dimensional time-frequency space that is comparable with the first order GFRFs, the second order GFRFs were averaged along the ridge direction $f_1 + f_2 = C_i$ with C_i the position of the ridge (e.g. $C_i = \pm$ 4Hz in Fig. 5 A) (He et al., 2013). The negative frequencies in the GFRF plots were introduced purely mathematically (similar to the negative frequencies introduced in a Fourier transformation). A summation of a positive frequency f_1 and a negative frequency f_2 can be understood as a subtraction between two positive frequencies in the input signal.

The gains of first- and second-order GFRFs (Fig. 5) show a low frequency peak or ridge at 3-4Hz during "tremor-on" periods and a peak at much higher frequency 8-11Hz during the "tremor-off" state for both cases. Similar peak and ridge positions of the first- and higher-order GFRFs can often be observed in a nonlinear system's analysis due to the same expression of the denominators in the GFRFs expression (as in (5)) (He et al., 2013). However, this does not mean the linear and nonlinear parts of the system have similar effects or contribute equally to the system's output. The OFRF analysis (Fig. 6) shows that the second-order nonlinear effects dominate and have the largest contribution to the output (LFP) frequency response.

The ridges in the second-order GFRF represent the transfer of energy from input spectral components to the output spectra at their summation, i.e. $f_1 + f_2 = C_i$, to produce strong intermodulation or harmonic effects. The results therefore indicate during "tremor-on" that if the summations of some frequency components in the EEG are close to the ridge frequency

range (i.e. close to 3 or 4Hz) they would be amplified in the output (i.e. thalamic LFP) frequency response or spectrum. Similarly, during "tremor-off" state, the frequency combinations at a higher range (i.e. close to 8.5 or 11Hz) would be amplified in the thalamic LFP. In patient 2 during tremor, the low frequency peaks in the first-order GFRF are not standing out as in the patient 1, but the ridges in the second-order GFRF are remarkable. Therefore, strong nonlinear effects were consistently observed in both cases.

The low frequency components (below 5Hz) during "tremor-on" and the higher frequency components (around 10Hz) during "tremor-off" in the thalamic LFP spectra (Fig. 2) are likely to be introduced from the second-order nonlinear effects when EEG is treated as the input. The results also explain and are consistent with the observations in the bispectral analysis; the QPCs presented in LFP bispectra can be introduced from the second-order intermodulation or harmonic effects of the nonlinear EEG-LFP 'system'. For example, the harmonics of the peaks in the bispectra during "tremor-on" (i.e. (2.3Hz, 2.3Hz), (1.7Hz, 1.7Hz)) are very close to the ridges observed in the second-order GFRFs (i.e. at around 4Hz and 3Hz) in both cases. Similar concordance between the bispectral QPC estimates and the second-order GFRFs are detected in the "tremor-off" state, again in both cases. The change of the QPC from lower to higher frequencies during the tremor and resting states could actually be due to the change of the ridge positions in the second-order GFRFs that affects the system's output frequency response.

Time delays (or phase lags) estimated from the second-order GFRFs during tremor states show delays exceeding 50ms (around the ridge frequency in the corresponding GFRF gain plots). The time delays estimated at the resting state are much shorter but again in the range of 20ms. The results imply the involvement of a complex multisynaptic pathway or loop generating the tremorogenic oscillations during tremor 'on', and such connectivity move to a higher frequency range when the tremor related central oscillations are switched "off".

Based on the GFRFs and model's input (EEG) spectrum, the model's output frequency response can also be computed according to (4), where the input spectrum is obtained from FFT. The model's overall output frequency response $Y(f)$ corresponds to a NARX model based LFP spectrum estimation. The advantage of such a nonlinear model based spectrum estimation is that the overall $Y(f)$ can be decomposed into contributions from linear and n^{th}-order nonlinear effects, i.e. $Y(f) = \sum_{n=1}^{M} Y_n(f)$, with respect to the input, in this instance the EEG recording.

The overall and the decomposed OFRFs of the thalamic LFPs of patient 1 during "tremor-on" and "tremor-off" states are shown in Fig. 6. The overall model based OFRFs in both states are consistent with the spectra estimation from a standard FFT (Fig. 2A and 2B) despite the third- and higher-order nonlinearities not being taken into account. These results demonstrate the accuracy of the nonlinear NARX model estimation and corresponding frequency domain mapping. The linear and second-order nonlinear decompositions show that during both "tremor-on" and "tremor-off" states, the second-order nonlinear effects dominate the OFRF of the thalamic LFPs. This result highlights the importance of nonlinear interactions in revealing and understanding the interactions between EEG and thalamic LFPs both during tremor and resting states.

4. Discussion

Activity about the usual tremor frequency and its first harmonic has been regularly observed previously in subcortical structures, often despite the complete absence of tremor (Brittain and Brown, 2013, 2014). An example of this is shown in the thalamic LFP power spectra (Fig. 2C and 2D) of our second case that does not show any unequivocal frequency differences between tremor active epochs and those at rest. On the other hand, in our first patient there is clearly higher power of low frequencies when the tremor is on and the tremor frequency and its first harmonic are visible on the power spectra of both thalamus and EMG. Coherence analysis between the ipsilateral frontocentral EEG and the thalamus shows only borderline significant, if at all, interactions between the two regions during "tremor-on", despite the fact that both are considered to be part of the same central oscillating motor network (Schnitzler et al., 2009, Raethjen and Deuschl, 2012).

With the use of linear association methodology and through the study of LFPs and thalamic single neurone activity, Marsden *et al*. and others (Marsden et al., 2000, Hua and Lenz, 2005) have found high coherence between Vim thalamus and EMG activity recorded during tremor. They showed a strong linear relationship around the frequency of the tremor. We demonstrate similar effects in both our essential tremor cases, with coherence values much above the 95% confidence limit estimated with a bootstrap method (Fig. 3C and 3D). Nevertheless, we did not observe a strong linear relationship between thalamus and cortical EEG with coherence (Fig. 3A and 3B) and one might erroneously deduce that there are no significant interactions between these two regions during tremor active periods. Brittain and Brown (Brittain and Brown, 2014) highlight in their recent work that this field of research has

suffered from a "reductionist view" in which function has been pursued in specific frequencies rather than in cross-frequency patterns of modulation. This view is further reinforced from a study in Parkinson's disease (López-Azcárate et al., 2010) that showed that beta activities in the high and low beta bands in the subthalamic nucleus demonstrate non-linear relationships. A few years prior to this, non-linear dopamine-dependent correlations were again demonstrated with subthalamic LFPs (Marceglia et al., 2006a).

Assessment of cross-frequency phase coupling with bispectral analysis of the thalamic LFPs (Fig. 4), in the herein-presented two cases, uncovers the fact that the thalamus as an output signal exhibits significant nonlinear behaviours. The interactions revealed with this approach show that entirely different frequencies are involved in the "tremor-on" versus "tremor-off" states, obvious even to untrained eyes (Fig. 4). However, the nonlinear effects on the thalamic LFP bispectra provide no clues as to the input/s in the system that could be generating these QPC effects, especially when multiple peaks are observed in the bispectra. This can make a bispectral result difficult to interpret and to compare under different conditions.

As a result of a more direct link between thalamic LFPs and EMG during tremor, the cortical rhythms were selected as the input and the thalamus as the output to our system and used to construct a novel nonlinear NARX model (Fig. 5). Additionally, this selection is also based on a nonlinear causality analysis between the EEG and LFPs using another recently developed nonlinear partial directed coherence (PDC) method (He et al., 2014). The results show stronger nonlinear causal effects from EEG to LFP, which further support the choice of treating the EEG as the input in our system. The nonlinear NARX model based analysis uncovers two distinct and not overlapping frequency "channels" of communication between Vim thalamus and the ipsilateral cortex, defining robustly "tremor-on" versus "tremor-off" states. The tremor active state is expressed by low frequency (around 3-4 Hz) nonlinear interactions while the resting state is dominated by alpha range (around 8.5-11Hz) nonlinear interactions (Fig. 5). The findings were remarkably similar in both our cases and were in keeping with the observations on the bispectral thalamic Vim LFP analysis.

Time delay estimates between thalamic LFP and EEG from the nonlinear part of the NARX model during tremor active states show delays exceeding 50ms, implying involvement of a multisynaptic pathway and/or a long loop within the tremorogenic oscillations. However, this provides no more specific information as to the subcortical areas participating in this loop. Such degree of delay is clearly beyond the lags inferred by direct white matter tracts connecting thalamus and cortex that are at most in the range of few

milliseconds (Walker et al., 2012). The time lags estimated at the resting state are much shorter but again in the range of 20ms implying a multisynaptic, albeit faster or shorter, pathway of functional connectivity between the two structures. Additionally, and remarkably in the resting state there is a shift of the peak of the interactions at a higher frequency range.

The importance of the nonlinear interactions between cortical and subcortical areas (the thalamus in this instance) during periods of tremor is emphasised by multiple levels of evidence in our approach: Firstly, the failure of coherence in revealing significant interactions. Secondly, the absence of clear linear components in the NARX model in the second case (Fig. 5C). Thirdly, and most importantly, the results in the model's output frequency response (Fig. 6) that displays the prominence of the nonlinear contribution of the model's input to the output signal, i.e. the Vim LFP spectrum. Finally, the ridge of the second-order GFRF of the NARX model shows findings, remarkably consistent with most of the QPC results in the bispectra for both cases, confirming that the cortical input plays a major role to these observations.

For the first time (to the best of our knowledge) we show with a novel parametric model based frequency domain analysis the importance of nonlinear dynamics in unveiling the interactions between thalamus and cortex. These findings might well not be a unique feature of essential tremor. As mentioned above, nonlinear effects have been previously reported in analysis of LFPs recorded from the subthalamic nucleus (Marceglia et al., 2006a, López-Azcárate et al., 2010) of patients with Parkinson's disease. In our two cases, a simple visual inspection of the bispectrum and the nonlinear model based analysis allows a clear differentiation between "tremor-on" versus "tremor-off" states in the frequency domain. This work provides evidence that information processing between cortical and subcortical regions does not exclusively involve activity in individual rhythms but also includes interactions between rhythms of different frequencies (Brittain and Brown, 2014). However, these phenomena appear to be undetectable without appropriate nonlinear analysis tools.

Therefore, we have shown that although there are strong linear effects between thalamus and muscle during tremor active periods, the same is not true between cortex and thalamus, both areas recognised previously to be part of the central tremor generating network in essential tremor. In our two cases, the dynamic interrelationship between cortex and thalamus can only be reliably unravelled when nonlinear methods are used. Such methodology may play a key role in revealing phenomena beyond the observational capabilities offered by the first order univariate and bivariate approaches such as spectral analysis and coherence. We demonstrate with clarity the advantages and the unique information revealed by a non-linear

approach in two patients with essential tremor. We need to further explore if this methodology can be used as a novel biomarker that can identify, exclusively based on central oscillations, periods when the tremor is active on larger number of patients with essential and other forms of tremor. Our nonlinear methodology might prove crucial for the understanding of the complex interactions between different constituents of the central motor network of centrally driven tremors. If our observations can be reproduced in larger cohorts, our approach could be used to activate on demand, high frequency thalamic deep brain stimulation and create a closed-loop device.

5. Conclusions

In this work, we introduce a nonlinear NARX modelling approach to identify the corticothalamic interactions in two patients with essential tremor. With this innovative methodology, we reveal that under "tremor-on" state the thalamic output shows significant nonlinear interactions at the frequency of the tremor around 4 Hz and time lags exceeding 50ms. The same analysis when the tremor is off shows interactions at much higher frequencies in the thalamic output at around 8-11Hz and associated time lags below 50ms. Thus, "tremor-on" versus "tremor-off" periods show non-overlapping frequencies and time lags in the non-linear domain of our model. The results also offer an explanation for the bispectral observations of QPC on the thalamic LFPs during both states, previously observed by other authors. We provide for the first time proof-of-concept of the importance of the nonlinear interactions between cortex and Vim thalamus in characterising this part of the central tremorogenic network in essential tremor. We need to explore further to what extend cross frequency nonlinear rather than single frequency linear interactions are required in characterising interrelationships between cortical and subcortical areas in centrally driven tremors, as this could offer an entirely new dimension in tremor research.

Appendix A.

The contributions of the pure input, output and cross-product non-linearities in (5) are given as

$$
\begin{aligned}
H_{n_u}(f_1,\ldots,f_n) &= \sum_{k_1,k_n=1}^{K} c_{0,n}(k_1,\ldots,k_n)e^{-j2\pi(f_1k_1+\cdots+f_nk_n)/f_s} \\
H_{n_{uy}}(f_1,\ldots,f_n) &= \sum_{q=1}^{n-1}\sum_{p=1}^{n-q}\sum_{k_1,k_{p+q}=1}^{K} c_{p,q}(k_1,\ldots,k_{p+q}) \\
&\quad \times H_{n-q,p}(f_1,\ldots,f_{n-q})e^{-j2\pi(f_{n-q+1}k_{n-q+1}+\cdots+f_{p+q}k_{p+q})/f_s} \\
H_{n_y}(f_1,\ldots,f_n) &= \sum_{p=2}^{n}\sum_{k_1,k_n=1}^{K} c_{0,n}(k_1,\ldots,k_n)H_{n,p}(f_1,\ldots,f_n)
\end{aligned}
\tag{A.1}
$$

The contribution of the pth-order non-linearity in $y(t)$ to the nth-order GFRF, $H_{n,p}(\cdot)$, can be recursively computed according to (Peyton Jones and Billings 1989) as

$$
H_{n,p}(\cdot) = \sum_{i=1}^{n-p+1} H_i(f_1,\ldots,f_i)H_{n-i,p-i}(f_{i+1},\ldots,f_n)e^{-j2\pi(f_1+\ldots+f_i)k_p/f_s} \tag{A.2}
$$

The above recursion finishes with p=1, where the $H_{n,1}(f_1,\ldots,f_n)$ is defined as

$$
H_{n,1}(f_1,\ldots,f_n) = H_n(f_1,\ldots,f_n)e^{-j2\pi(f_1+\ldots+f_i)k_1/f_s} \tag{A.3}
$$

References

Billings SA (2013) Nonlinear system identification : NARMAX methods in the time, frequency, and spatio-temporal domains: John Wiley & Sons.

Billings SA, Chen S, Korenberg MJ (1989) Identification of Mimo Non-Linear Systems Using a Forward-Regression Orthogonal Estimator. Int J Control 49:2157-2189.

Billings SA, Tsang KM (1989) Spectral-Analysis for Non-Linear Systems .2. Interpretation of Non-Linear Frequency-Response Functions. Mech Syst Signal Pr 3:341-359.

Billings SA, Voon WSE (1983) Structure detection and model validity test in the identification of nonlinear systems. IEE Proceedings, Pt D: Control Theory and Applications 130:193-199.

Brittain JS, Brown P (2013) The many roads to tremor. Exp Neurol 250:104-107.

Brittain JS, Brown P (2014) Oscillations and the basal ganglia: motor control and beyond. Neuroimage 85 Pt 2:637-647.

Chen S, Billings SA, Luo W (1989) Orthogonal least squares methods and their application to nonlinear system identification. Int J Control 50:1873-1896.

Deuschl G, Raethjen J, Hellriegel H, Elble R (2011) Treatment of patients with essential tremor. Lancet Neurol 10:148-161.

Govindan RB, Raethjen J, Arning K, Kopper F, Deuschl G (2006) Time delay and partial coherence analyses to identify cortical connectivities. Biological cybernetics 94:262-275.

Halliday DM, Conway BA, Farmer SF, Shahani U, Russell AJ, Rosenberg JR (2000) Coherence between low-frequency activation of the motor cortex and tremor in patients with essential tremor. Lancet 355:1149-1153.

He F, Billings SA, Wei HL, Sarrigiannis PG (2014) A nonlinear causality measure in the frequency domain: Nonlinear partial directed coherence with applications to EEG. J Neurosci Meth 225:71-80.

He F, Billings SA, Wei HL, Sarrigiannis PG, Zhao Y (2013) Spectral Analysis for Nonstationary and Nonlinear Systems: A Discrete-Time-Model-Based Approach. Biomedical Engineering, IEEE Transactions on 60:2233-2241.

He F, Wei HL, Billings SA (2015) Identification and frequency domain analysis of non-stationary and nonlinear systems using time-varying NARMAX models. Int J Syst Sci 46:2087-2100.

Hellwig B, Häussler S, Lauk M, Guschlbauer B, Köster B, Kristeva-Feige R, Timmer J, Lücking CH (2000) Tremor-correlated cortical activity detected by electroencephalography. Clin Neurophysiol 111:806-809.

Hellwig B, Häussler S, Schelter B, Lauk M, Guschlbauer B, Timmer J, Lücking CH (2001) Tremor-correlated cortical activity in essential tremor. Lancet 357:519-523.

Hellwig B, Schelter B, Guschlbauer B, Timmer J, Lücking CH (2003) Dynamic synchronisation of central oscillators in essential tremor. Clin Neurophysiol 114:1462-1467.

Hirai T, Miyazaki M, Nakajima H, Shibazaki T, Ohye C (1983) The correlation between tremor characteristics and the predicted volume of effective lesions in stereotaxic nucleus ventralis intermedius thalamotomy. Brain 106 (Pt 4):1001-1018.

Hua SE, Lenz FA (2005) Posture-related oscillations in human cerebellar thalamus in essential tremor are enabled by voluntary motor circuits. J Neurophysiol 93:117-127.

Hubble JP, Busenbark KL, Wilkinson S, Penn RD, Lyons K, Koller WC (1996) Deep brain stimulation for essential tremor. Neurology 46:1150-1153.

Jones EG (2007) The Thalamus. Cambridge, UK: Cambridge Univ. Press.
Jones JCP, Billings SA (1989) Recursive Algorithm for Computing the Frequency-Response of a Class of Non-Linear Difference Equation Models. Int J Control 50:1925-1940.
Lang ZQ, Billings SA (1996) Output frequency characteristics of nonlinear systems. Int J Control 64:1049-1067.
Lehnertz K (2008) Epilepsy and nonlinear dynamics. J Biol Phys 34:253-266.
Leontaritis IJ, Billings SA (1985) Input-output parametric models for nonlinear systems, part I: deterministic nonlinear systems. Int J Control 41:303-328.
López-Azcárate J, Tainta M, Rodríguez-Oroz MC, Valencia M, González R, Guridi J, Iriarte J, Obeso JA, Artieda J, Alegre M (2010) Coupling between beta and high-frequency activity in the human subthalamic nucleus may be a pathophysiological mechanism in Parkinson's disease. J Neurosci 30:6667-6677.
Lyons KE, Pahwa R (2004) Deep brain stimulation and essential tremor. J Clin Neurophysiol 21:2-5.
Marceglia S, Foffani G, Bianchi AM, Baselli G, Tamma F, Egidi M, Priori A (2006a) Dopamine-dependent non-linear correlation between subthalamic rhythms in Parkinson's disease. J Physiol 571:579-591.
Marceglia S, Foffani G, Bianchi AM, Baselli G, Tamma F, Egidi M, Priori A (2006b) Dopamine-dependent non-linear correlation between subthalamic rhythms in Parkinson's disease. J Physiol-London 571:579-591.
Marsden JF, Ashby P, Limousin-Dowsey P, Rothwell JC, Brown P (2000) Coherence between cerebellar thalamus, cortex and muscle in man: cerebellar thalamus interactions. Brain 123:1459-1470.
Muthuraman M, Heute U, Arning K, Anwar AR, Elble R, Deuschl G, Raethjen J (2012) Oscillating central motor networks in pathological tremors and voluntary movements. What makes the difference? NeuroImage 60:1331-1339.
Nikias CL, Raghuveer MR (1987) Bispectrum Estimation - a Digital Signal-Processing Framework. P Ieee 75:869-891.
Orth RC, Sinha P, Madsen EL, Frank G, Korosec FR, Mackie TR, Mehta MP (1999) Development of a unique phantom to assess the geometric accuracy of magnetic resonance imaging for stereotactic localization. Neurosurgery 45:1423-1429.
Papanastassiou V, Rowe J, Scott R, Silburn P, Davies L, Aziz T (1998) Use of the Radionics Image Fusiontrade mark and Stereoplantrade mark programs for target localization in functional neurosurgery. Journal of clinical neuroscience : official journal of the Neurosurgical Society of Australasia 5:28-32.
Raethjen J, Deuschl G (2012) The oscillating central network of Essential tremor. Clin Neurophysiol 123:61-64.
Raethjen J, Govindan RB, Kopper F, Muthuraman M, Deuschl G (2007) Cortical involvement in the generation of essential tremor. Journal of Neurophysiology 97:3219-3228.
Schnitzler A, Münks C, Butz M, Timmermann L, Gross J (2009) Synchronized brain network associated with essential tremor as revealed by magnetoencephalography. Mov Disord 24:1629-1635.
Siu KL, Ahn JM, Ju K, Lee M, Shin K, Chon KH (2008) Statistical approach to quantify the presence of phase coupling using the bispectrum. Ieee T Bio-Med Eng 55:1512-1520.
Theiler J, Eubank S, Longtin A, Galdrikian B, Farmer JD (1992) Testing for Nonlinearity in Time-Series - the Method of Surrogate Data. Physica D 58:77-94.
Vaillancourt DE, Sturman MM, Verhagen Metman L, Bakay RA, Corcos DM (2003) Deep brain stimulation of the VIM thalamic nucleus modifies several features of essential tremor. Neurology 61:919-925.

Walker HC, Huang H, Gonzalez CL, Bryant JE, Killen J, Knowlton RC, Montgomery EB, Jr., Cutter GC, Yildirim A, Guthrie BL, Watts RL (2012) Short latency activation of cortex by clinically effective thalamic brain stimulation for tremor. Mov Disord 27:1404-1412.

Wang Z, Huang Y, Wang S, Green A, Aziz T, Stein J (2014) Tremor dependant nonlinear interaction in deep brain local field potentials of Parkinson's disease. In: Biomedical Engineering and Informatics (BMEI), 2014 7th International Conference on, pp 399-404.

Worden K (1998) Confidence bounds for frequency response functions from time series models. Mech Syst Signal Pr 12:559-569.

Zhang D, Snyder AZ, Fox MD, Sansbury MW, Shimony JS, Raichle ME (2008) Intrinsic Functional Relations Between Human Cerebral Cortex and Thalamus. Journal of Neurophysiology 100:1740-1748.

Figures & Tables:

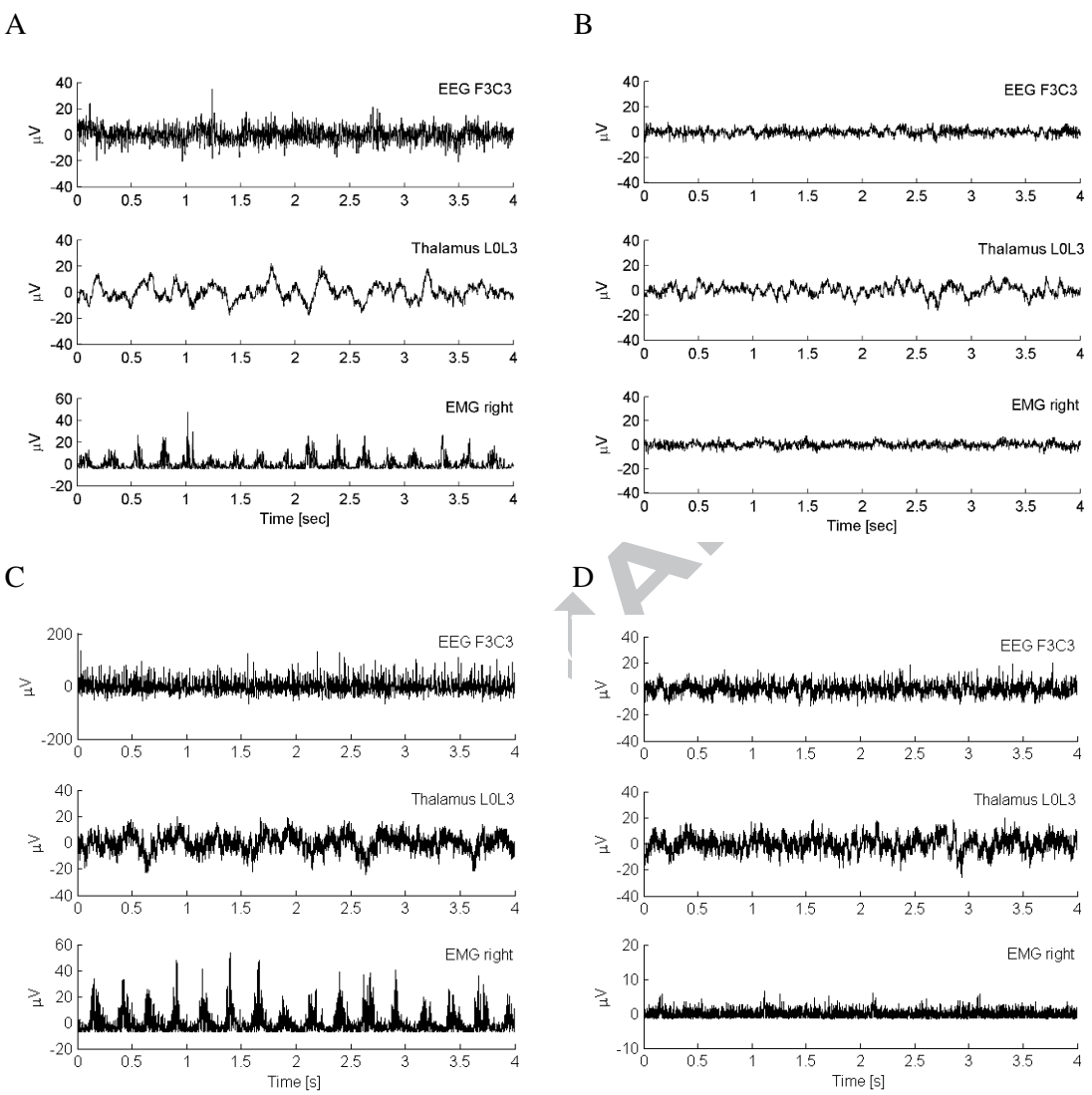

Fig .1. Time series of EEG, thalamic LFP, and EMG recordings for patient 1 during (A) tremor and (B) resting states, and patient 2 during (C) tremor and (D) resting states. EMG recordings shown are from the right triceps brachii.

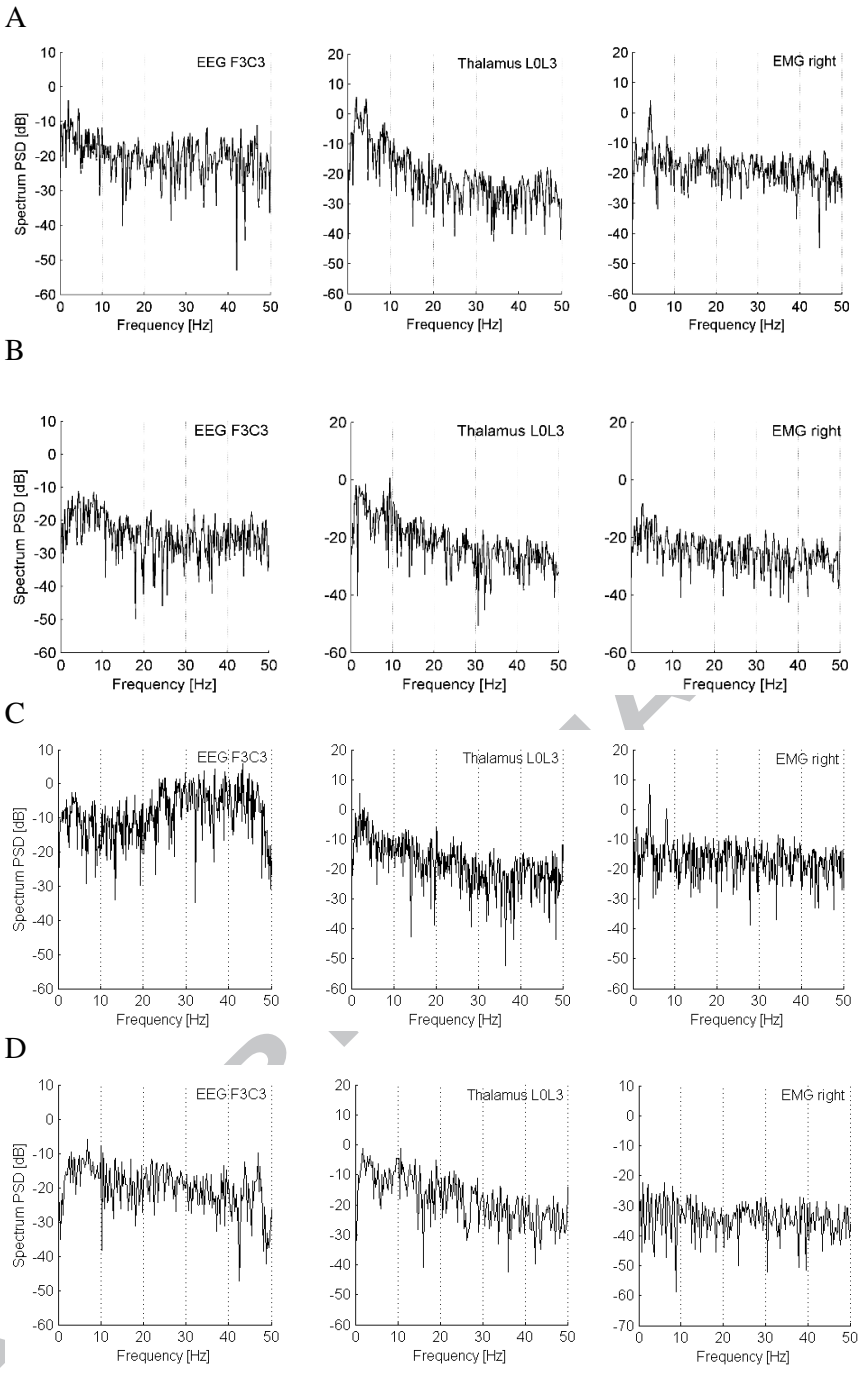

Fig. 2. Power spectra from two patients with essential tremor. (A) EEG, LFPs and EMG from the right triceps brachii during "tremor-on" state in patient 1. (B) EEG, LFPs and EMG from the right triceps brachii during "tremor-off" state in patient 1. (C) and (D) show the same channels for tremor on and off states, respectively, for patient 2.

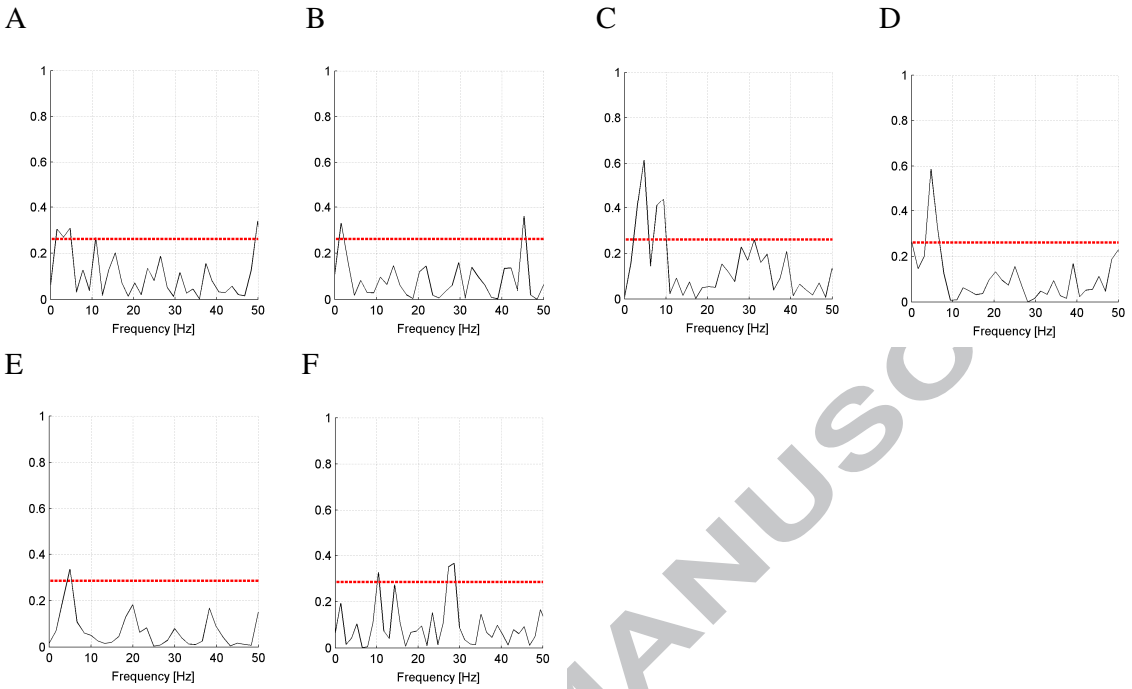

Fig. 3. Coherence between EEG and thalamic LFP for (A) patient 1 and (B) patient 2, between EMG and thalamic LFP for (C) patient 1 and (D) patient 2, and between EEG and EMG for (E) patient 1 and (F) patient 2 during "tremor-on" state.

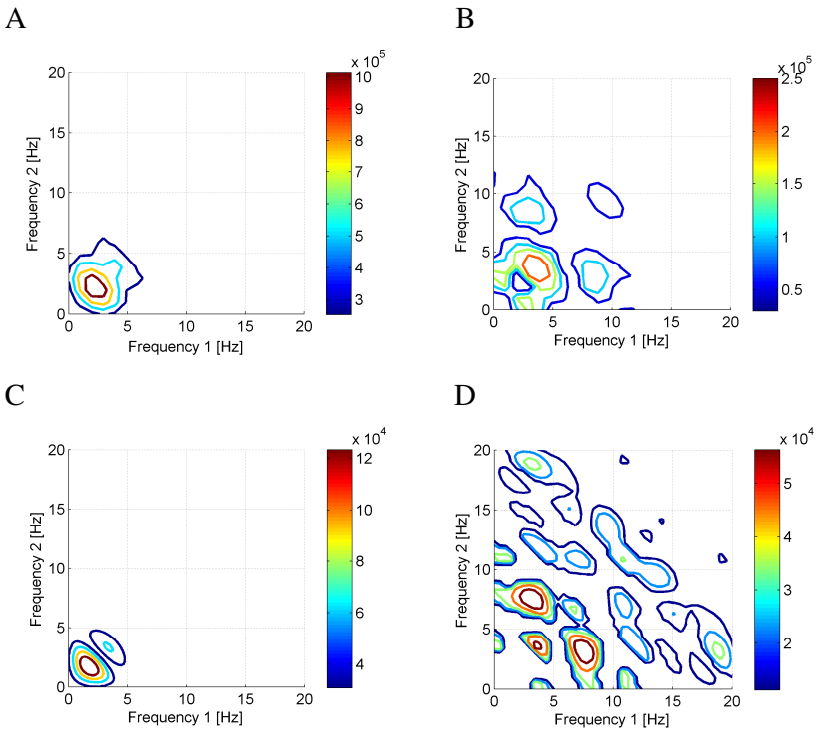

Fig. 4. Bispectral analysis of thalamic Vim LFP for patient 1 during (A) tremor and (B) resting states, and patient 2 during (C) tremor and (D) resting states.

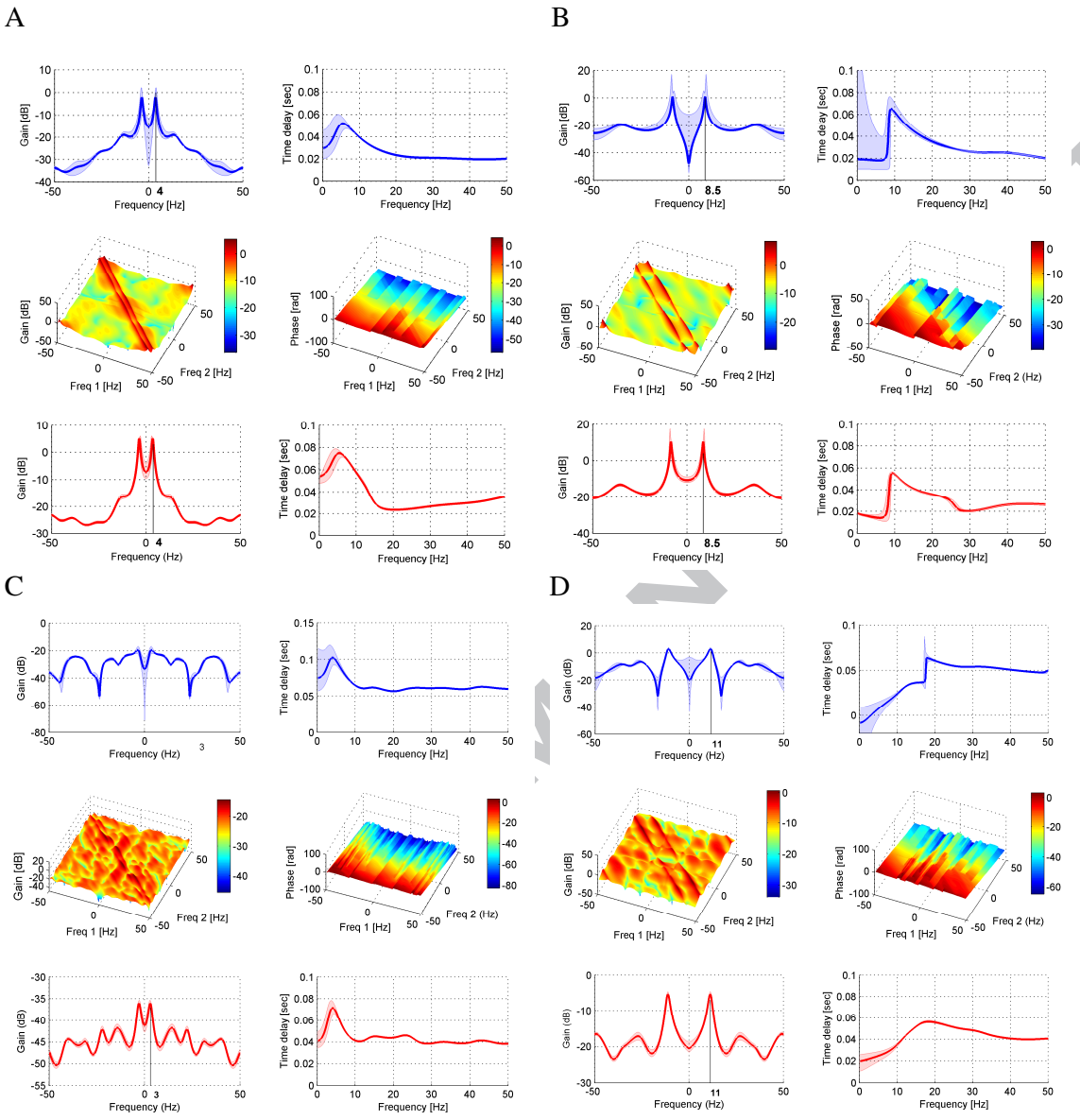

Fig. 5. GFRFs of patient 1 during (A) "tremor-on" and (B) "tremor-off" states, and patient 2 during (C) "tremor-on" and (D) "tremor-off" states. In each subfigure, the GFRFs are shown in the following order: first-order (upper trace, in blue), second-order (middle trace) and averaged second-order (lower trace, in red). The gain plots are shown on the left of each subfigure and phase lags on the right. The 95% confidence interval estimates are shown in shaded regions. The confidence intervals with respect to the linear first-order GFRFs have a much higher scatter in comparison to the nonlinear GFRF estimates.

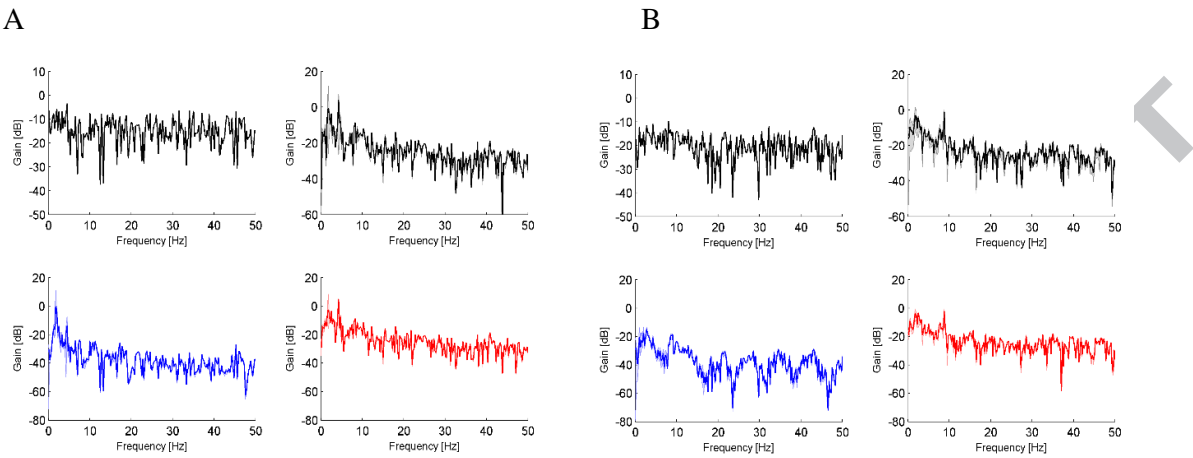

Fig. 6. Output frequency response functions (OFRFs) of the thalamic LFP of patient 1 (A) during "tremor-on" and (B) "tremor-off" states. In each subfigure, the upper-left plot is the spectrum of EEG recording from the FFT and the upper-right plot shows the overall OFRF $Y(f)$ of thalamic LFP; lower-left plot (in blue) shows the linear contribution to the OFRF $Y_1(f)$ and the lower-right plot (in red) shows the second-order nonlinear contribution to the OFRF $Y_2(f)$.

Table 1. DBS parameters and electrode placement

Parameters	Patient 1	Patient 2
Age at surgery	64	60
Gender	F	F
Pre-op FTM*	49/144	63/144
Post-op FTM*	13/144	18/144
Right Vim DBS**		
Contacts	1 (+), 2 (-)	3 (-), 2 (+)
Frequency (Hz)	130	130
Pulse width (µS)	90	120
Amplitude (V)	0.7	3.5
Left Vim DBS **		
Contacts	0 (+), 1(-)	1 and 2 (-), 0 (+)
Frequency (Hz)	130	130
Pulse width (µS)	180	210
Amplitude (V)	1.3	1.5
Right Vim DBS Coordinates (AP, LT)	AP -0.4 LT 10.1	AP -3.9 LT 14.7
Left Vim DBS Coordinates (AP, LT)	AP -2.3 LT 10.0	AP -3.1 LT 13.5
Mean for AP and LT Coordinates (+/-1SD)	AP and LT-2.4 (1.5)	AP and LT 12.1 (2.4)

* FTM: Fahn -Tolosa Marin tremor rating scale
** Ideal stimulation contacts selected during EEG/EMG/LFP recordings
AP: anteroposterior, LT: lateral